Myocardial Infarction Activates CCR2+ Hematopoietic Stem and Progenitor Cells

Supplemental Information

Dutta et al.: Myocardial infarction activates CCR2^{+} hematopoietic stem and progenitor cells

Corresponding authors: Matthias Nahrendorf and Partha Dutta
Center for Systems Biology
185 Cambridge Street
Boston, MA 02114
Tel: (617) 643-0500
Fax: (617) 643-6133
mnahrendorf@mgh.harvard.edu
dutta.partha@mgh.harvard.edu

SUPPLEMENTAL FIGURES

Figure S1

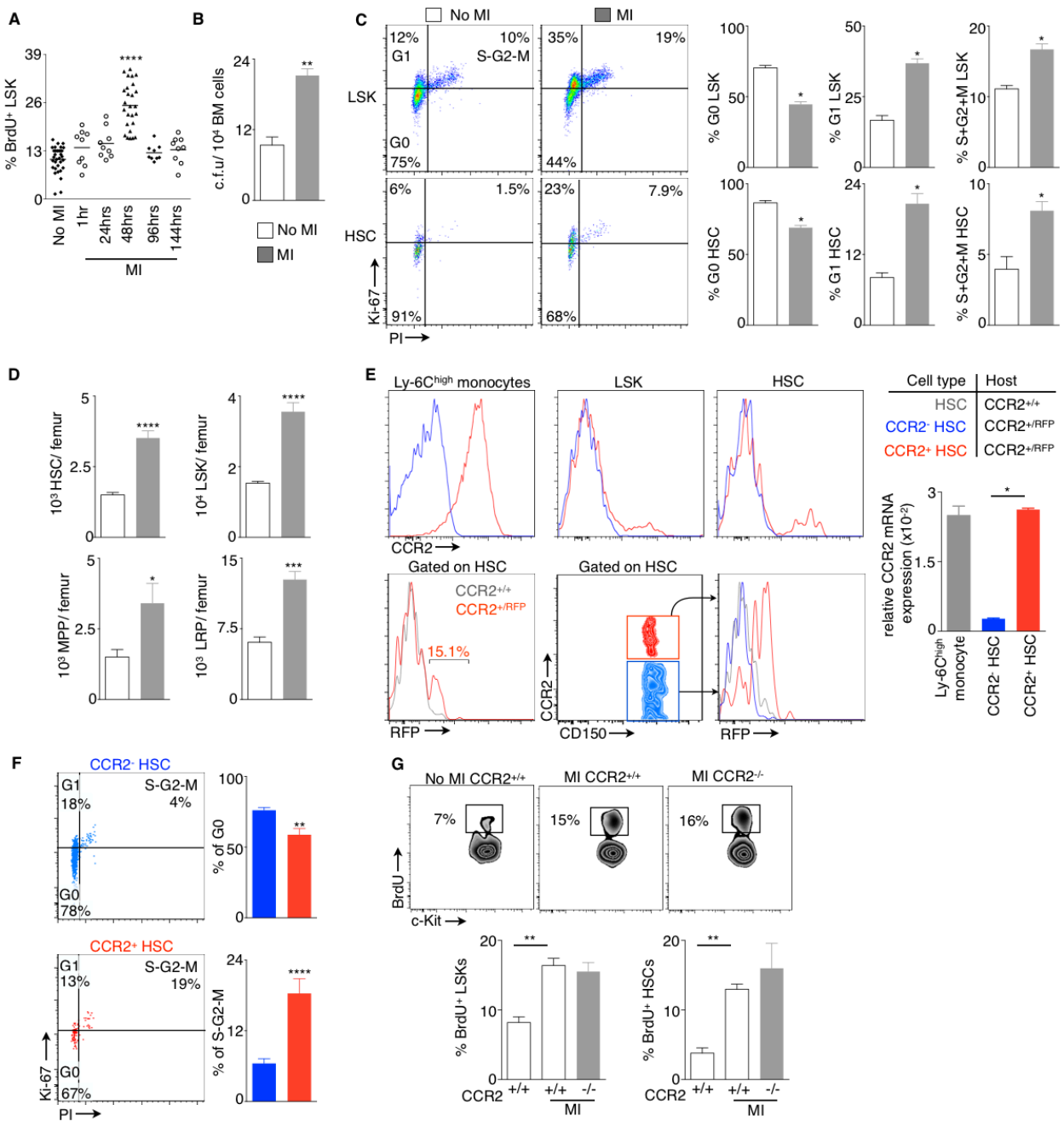

Figure S1. HSC and CCR2 after MI, related to Figure 1
(A) LSK proliferation measured by BrdU incorporation with flow cytometry at steady state (no MI) and different time points after MI (n=8-29 per group).
(B) Number of colony-forming units per 10^4 bone marrow cells collected from mice at steady state and 3 days after MI (n=5 per group).

(C) Flow cytometric plots show LSK and HSC at different phases of the cell cycle on day 2 after MI. The bar graphs depicts quantification of % of LSK and HSC at different phases of the cell cycle (n=4-5 per group).
(D) Quantification of LSK, HSC, MPP and LRP in the femur on day 3 after MI (n=7-15 per group).
(E) Flow cytometric plots showing CCR2 expression on Ly-6C^{high} monocytes, LSK and HSC, and red fluorescent protein (RFP) expression on bone marrow HSC of wild type (CCR2$^{+/+}$) and CCR2$^{+/RFP}$ mice on protein level by FACS and mRNA level by PCR in FACS-isolated cells (n=3-4 per group).
(F) Cell Cycle analysis of HSC: Flow cytometric plots show CCR2^{+} and CCR2^{-} HSC at different phases of the cell cycle in the steady state. The bar graphs depict quantification of % of CCR2^{+} and CCR2^{-} HSCs at different phases of the cell cycle (n=7-9 per group).
(G) BrdU incorporation by HSC in wild type and CCR2$^{-/-}$ mice 48 hours after MI. Bar graphs depict % of BrdU^{+} LSK and HSC (n=4-14 per group). Data are shown as mean ± SEM, * $P < 0.05$, ** $P < 0.01$, **** $P < 0.0001$.

Figure S2

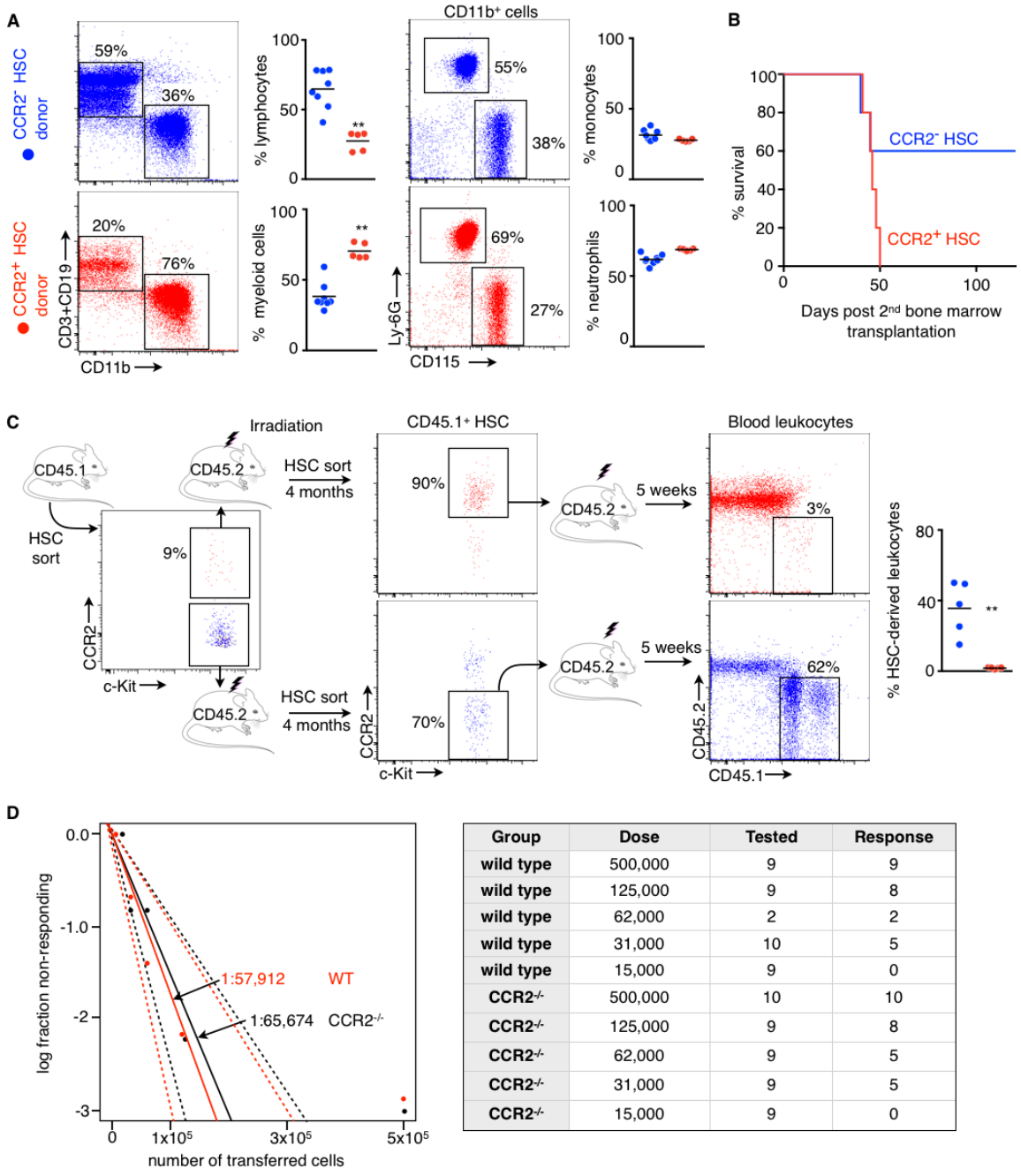

Group	Dose	Tested	Response
wild type	500,000	9	9
wild type	125,000	9	8
wild type	62,000	2	2
wild type	31,000	10	5
wild type	15,000	9	0
CCR2$^{-/-}$	500,000	10	10
CCR2$^{-/-}$	125,000	9	8
CCR2$^{-/-}$	62,000	9	5
CCR2$^{-/-}$	31,000	9	5
CCR2$^{-/-}$	15,000	9	0

Figure S2. Bone marrow chimerism after HSC transplantation, related to Figure 3.
(A) Chimerism in bone marrow lymphocytes, myeloid cells, and monocytes and neutrophils after primary transplantation of either 100 CCR2^{+} or 100 CCR2^{-} CD150^{+} CD48^{-} LSK.
(B) Survival after secondary transplantation of CCR2^{+} versus CCR2^{-} CD150^{+} CD48^{-} LSK (n=5 per group).
(C) Leukocyte chimerism in secondary recipients of either 100 CCR2^{+} or 100 CCR2^{-} CD150^{+} CD48^{-} LSK.
(D) Limiting dilution assay comparing the frequency of functional HSC in wild type and CCR2$^{-/-}$ bone marrow ($p = 0.74$ for difference in cell frequency). Multi-lineage blood chimerism of 0.1%

or higher served as cut off value to determine responders. Table lists dilution steps, numbers of mice analyzed 4 months after HSC transfer, and number of responders.
Data are shown as mean ± SEM, ** $P < 0.01$.

Figure S3

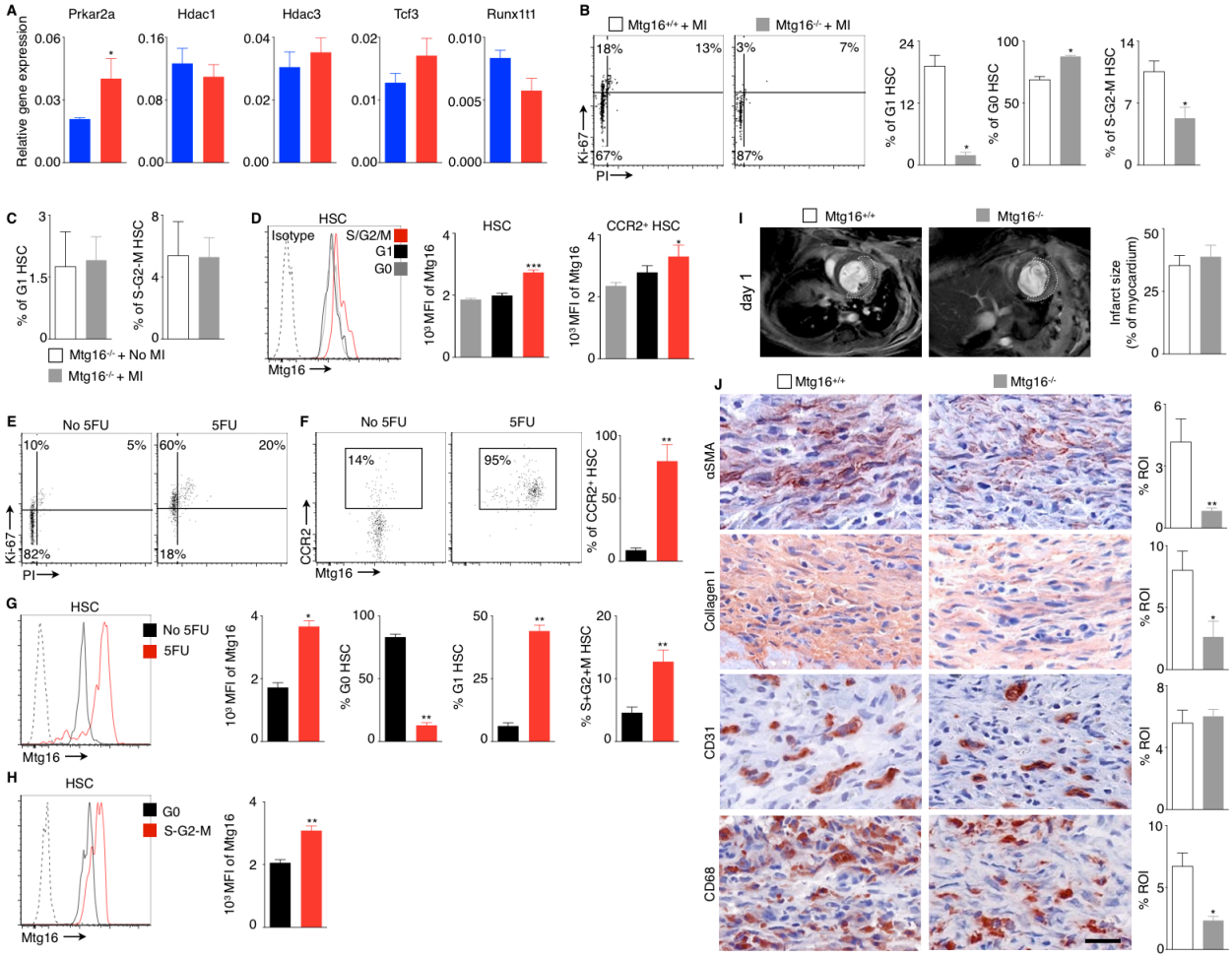

Figure S3. Mtg16 in HSPC, related to Figure 4.
(A) Bar graphs show mRNA expressions of Mtg16 targets relative to Gapdh Ct values in the HSC subsets (n=3-11 per group).
(B) Reduced HSC proliferation in *Mtg16*$^{-/-}$ mice on day 2 after MI when compared to wild type mice with MI (n=4 per group).
(C) In *Mtg16*$^{-/-}$ mice, HSC do not increase proliferation after coronary ligation when compared to steady state *Mtg16*$^{-/-}$ mice without MI (n=3-4 per group).
(D) Mtg16 expression in steady-state wild type HSC during various cell cycle phases (n=10 per group).
(E) HSC proliferation after 5FU challenge. The majority of HSC express CCR2 48 hrs after 5FU
(F) (n=5 per group), and these cells increase expression of Mtg16 (G) while entering active phases of the cell cycle (n=5 per group). Dotted line in histogram shows staining control.
(H) Mtg16 expression increases in proliferating CCR2$^{-/-}$ HSC on day 2 after MI (n=6 per group).
(I) Baseline MRI on day 1 after MI used delayed gadolinium enhancement to measure infarct size (n=6-7 per group).
(J) Immunoreactive staining for wound healing biomarkers on day 7 after MI in wild type and *Mtg16*$^{-/-}$ mice (n=5 per group).
Data are mean ± SEM, * $P < 0.05$, ** $P < 0.01$.

Figure S4

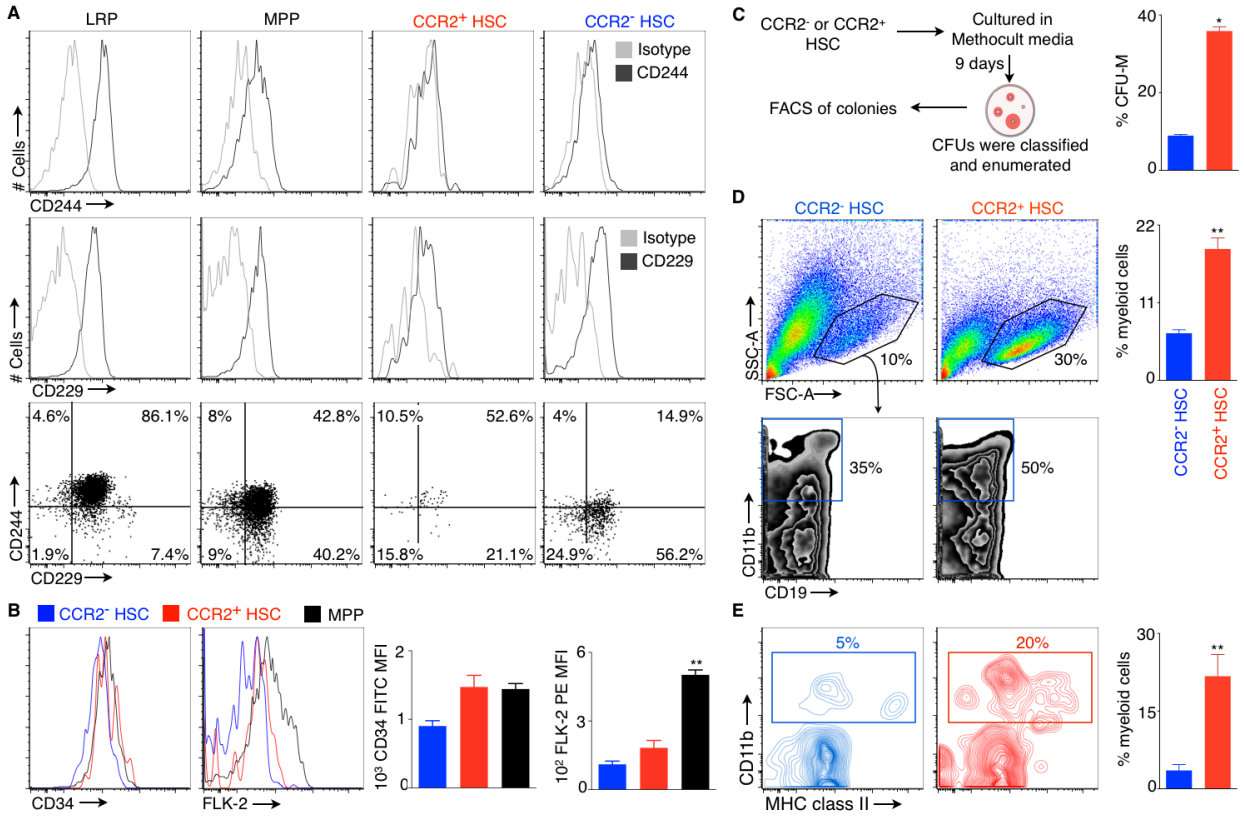

Figure S4. Quiescence and lineage bias, related to Figure 5
(A) Analysis of Slamf3 (CD229) and Slamf4 (CD244) expression. Flow cytometric plots show CD244 and CD229 expression on LRP, MPP, CCR2$^-$ and CCR2$^+$ CD150$^+$ CD48$^-$ LSK.
(B) Expression of CD34 and FLK-2 in respective CD48$^-$ CD150$^+$ CD150$^+$ CD48$^-$ LSK subsets and in CD48$^-$ CD150$^-$ multipotent progenitors (MPP) (n=5 per group).
(C) In vitro culture of CCR2$^+$ and CCR2$^-$ CD150$^+$ CD48$^-$ LSK. Left panel: Flow chart depicting experimental design. Right panel: The bar graph shows % of colony forming units for myeloid cells (CFU-M) derived from CCR2$^+$ and CCR2$^-$ CD150$^+$ CD48$^-$ LSK after culturing for 9 days in semisolid Methocult media (n=4 per group).
(D) Percentage of myeloid cells derived from CCR2$^+$ and CCR2$^-$ CD150$^+$ CD48$^-$ LSK cultured in methocult media (n=4-5 per group). Myeloid cell % was obtained by multiplying % of leukocytes (upper plots) with % of CD11b+ cells (lower plots).
(E) Percentage of myeloid cells derived from CCR2$^+$ and CCR2$^-$ CD150$^+$ CD48$^-$ LSK after culturing for 7 days in liquid media (n=5 per group). Data are shown as mean ± SEM, * $P < 0.05$, ** $P < 0.01$.

Figure S5

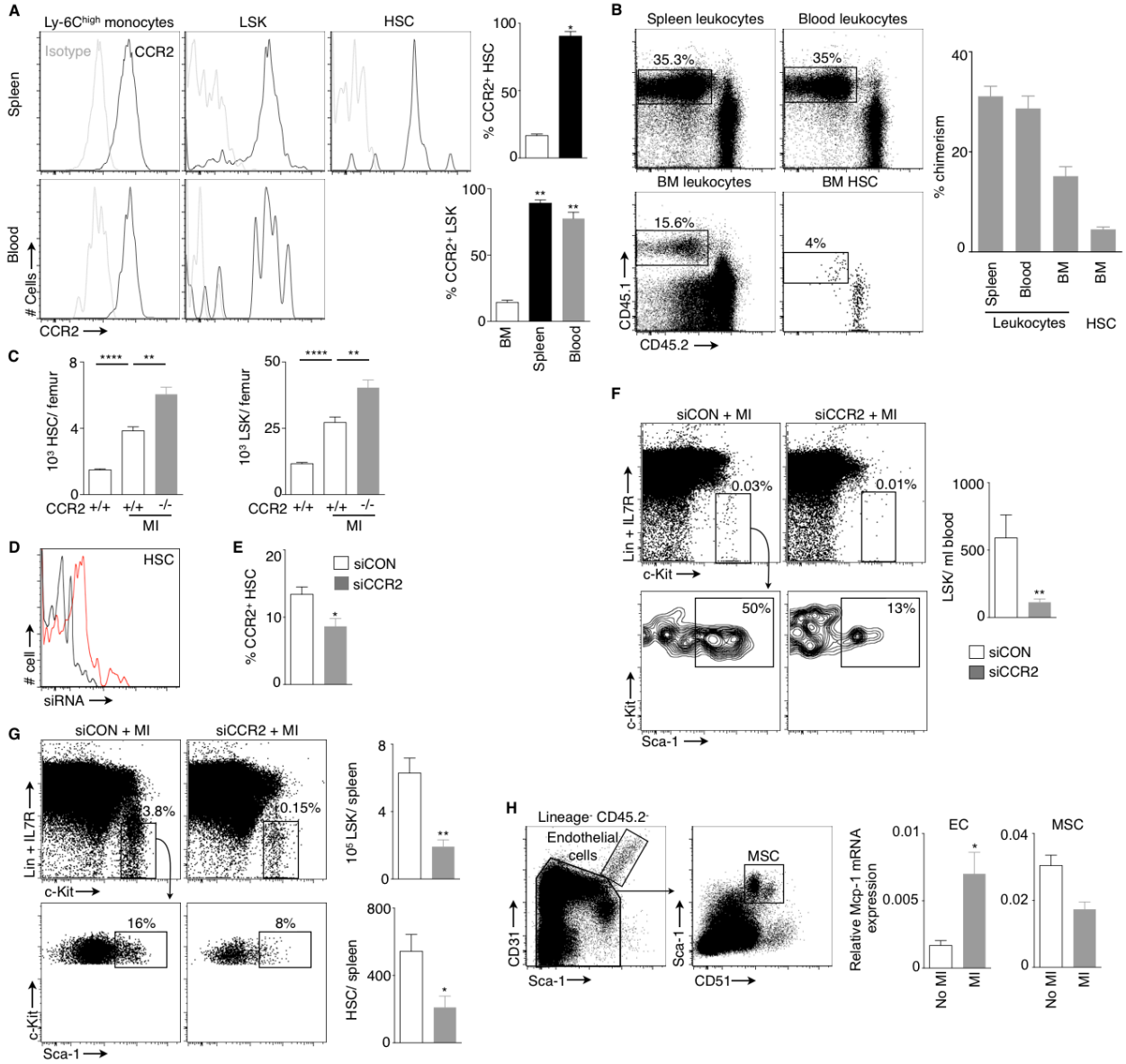

Figure S5. CCR2 expression and HSC migration, related to Figure 6

(A) CCR2 expression on blood and splenic HSC and LSK. The flow plots depict CCR2 expression on blood and splenic monocytes, LSK and HSC. The bar graphs represent % of $CCR2^+$ HSC and LSK in the bone marrow, spleen and blood (n=5-6 per group).

(B) Chimerism after 5 weeks of parabiosis in splenic, blood and bone marrow leukocytes and bone marrow HSC after 5 weeks of parabiosis (n=5 per group).

(C) Bone marrow retention of HSC in $CCR2^{-/-}$ mice. Flow cytometric enumeration of HSC and LSK in the femur in wild type and $CCR2^{-/-}$ mice in steady state and day 3 after MI (n=5-10 per group).

(D) Uptake of nanoparticle encapsulated, fluorochrome labelled siRNA after intravenous injection by bone marrow HSC.

(E) Percentage of $CCR2^+$ HSPC in the bone marrow after knocking down CCR2 with siRNA (siCON: control siRNA, siCCR2: siRNA targeting CCR2) (n=4-5 per group).

(F) FACS quantification of blood LSK after CCR2 silencing on day 4 after MI (n=6-8 per group).

(G) FACS quantification of splenic LSK and HSC after CCR2 silencing on day 4 after MI (n=5-7 per group).
(H) Expression of the CCR2 ligand Mcp-1 in cells flow-sorted from the bone marrow on day 4 after MI (EC, endothelial cells, MSC, mesenchymal stem cells). Data are shown as mean ± SEM, * $P < 0.05$, ** $P < 0.01$.

Figure S6.

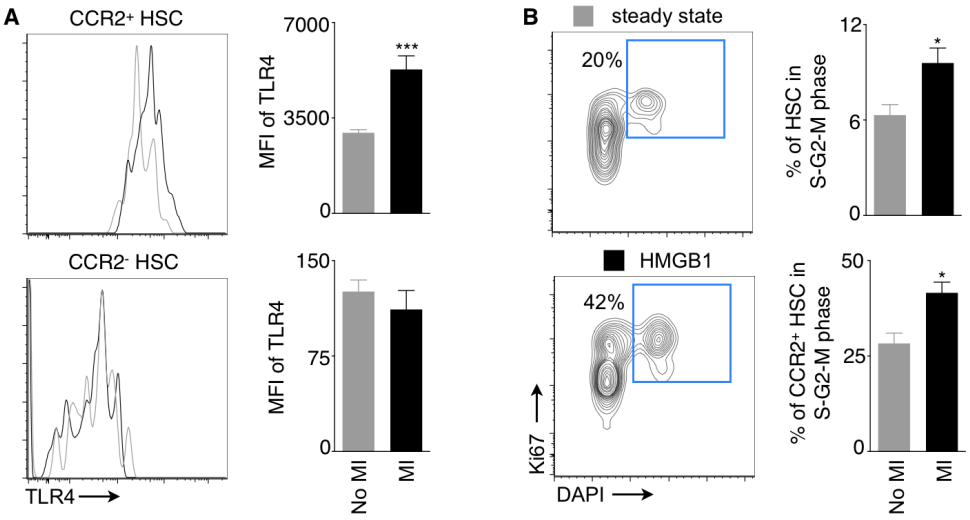

Figure S6, Expression of TLR4 and response to HMGB1, related to Figure 7.
(A) TLR4 expression on CCR2^{+} and CCR2^{-} CD150^{+} CD48^{-} LSK on day 2 after MI (n=7-10).
(B) CCR2^{+} HSPC proliferation 2 days after HMGB1 injection (n=5).
All data are shown as mean ± SEM. Statistical significance was determined by Mann-Whitney test. * $P < 0.05$, *** $P < 0.001$.

Table S1. Patient characteristics, related to Figure 2

Patient ID	Age	Sex	Surgery
1	51	male	CABG (Day 3 AMI)
2	69	male	CABG (Day 3 AMI)
3	84	male	CABG, Aortic Valve Replacement (Day 6 AMI)
4	62	male	CABG, Mitral and Tricuspid Valve Repair
5	65	male	Composite Aortic Root Replacement

CABG: Coronary Artery Bypass Grafting, AMI: Acute Myocardial Infarction

Legend Table S2, related to Figure 3 (see separate excel file)
Differentially expressed genes between $CCR2^{+}$ and $CCR2^{-}$ HSC at a false discovery rate cutoff of 10%. At this cutoff, only genes that are downregulated in $CCR2^{+}$ reached significance (negative d-values).

SUPPLEMENTAL EXPERIMENTAL PROCEDURES

Organ harvesting and tissue processing

Blood was drawn via cardiac puncture. Red blood cell lysis was performed with 1x RBC lysis buffer (BioLegend). Before harvesting the heart, animals were flushed with ice cold PBS through the left ventricle. Hearts were minced in digestion mixture containing 450 U/ml collagenase I, 125 U/ml collagenase XI, 60 U/ml DNase I, and 60 U/ml hyaluronidase (Sigma-Aldrich) and incubated at 37^{o} C at 750 rpm for 1 hour. Digestion was stopped with 10ml FACS buffer (PBS with 0.5% bovine serum albumin and 1% fetal bovine serum), and the cells were passed through 40μ filters to obtain single cell suspension. Spleens were minced in FACS buffer and passed through 40μ filters. Splenocytes were treated with 1x RBC lysis buffer to remove red blood cells. Femurs were flushed with ice cold FACS buffer.

Analysis of human bone marrow

Patient studies were conducted in accordance with the Declaration of Helsinki. The study protocol was approved by the Massachusetts General Hospital Internal Review Board. Patients having myocardial infarction or undergoing valve surgeries were identified. Patients scheduled to undergo cardiac surgery by sternotomy were informed of the study goals and methodologies, and consented if they wished to participate. In the operating room, after a midline sternotomy was performed, a small sample of bone marrow was collected from the already severed edge of the exposed sternum. The sample was transferred from the OR on ice, washed in Iscove's culture medium, resuspended in freezing medium containing 10% DMSO, and stored in liquid nitrogen at a concentration of 2-10 million cells/mL until it was thawed for immunostaining and analysis by flow cytometry. After thawing, the cells were washed once with RPMI and FBS (1:1) followed by another wash with FACS buffer (PBS with 1% FBS and 0.5% BSA). The cells were stained with biotinylated lineage antibodies comprising of anti-human CD2 (RPA-2.10), CD3 (HIT3a), CD4 (RPA-T4), CD7 (124-1D1), CD8 (RPA-T8), CD10 (SN5c), CD11b (ICRF44), CD14

(HCD14), CD19 (HIB19), CD20 (2H7) and CD56 (HCD56). This was followed by a secondary staining with anti-human CD90 (5E10), CCR2 (K036C2), CD38 (HIT2), CD34 (8G12) and CD45RA (MEM-56). Intracellular staining with anti-human Ki-67 (6H6) was performed using eBioscience intracellular staining protocol. HSC were identified as Lineage^{low} CD34^{high} CD38^{low} CD45RA^{low} CD90^{high} (Pang et al., 2011).

Proliferation assays

Mice were injected with 1 mg BrdU 24 hours before collecting organs, and intracellular BrdU staining was be performed using BrdU flow kits (BD Pharmingen). The cell cycle state was assessed with Ki-67 and propidium iodide staining. Quiescent cells (G0: Ki-67^{-} PI^{low}) and proliferating cells (G1: Ki-67^{+} PI^{low}, S-G2-M: Ki67^{+} PI^{high}) were enumerated using an LSRII.

Fluorescent-activated cell sorting (FACS)

All long bones and the spine were harvested in ice cold FACS buffer. Single cells were prepared after grinding the bones with a mortar and pestle. Cells were stained with biotinylated antibodies against lineage markers as described above followed by incubation with streptavidin microbeads (Miltenyi). The unconjugated cells, which were enriched for hematopoietic stem and progenitor cells, were separated using magnetic columns (Miltenyi). The enriched cells were stained with the antibodies described above. CCR2^{+} , CCR2^{-} CD150^{+} CD48^{-} LSK and MPP were sorted using a FACSAria IIu cell sorter (BD Biosciences).

Bone marrow reconstitution and limiting dilution assay

For competitive bone marrow reconstitution, GFP^{+} B6 mice were lethally irradiated (10 Gy) and reconstituted with 100 CCR2^{-} CD150^{+} CD48^{-} LSK, 100 CCR2^{+} CD150^{+} CD48^{-} LSK and 200,000 BM cells obtained from

GFP^{+} B6 mice. For radiation protection assays, CD45.2 mice were lethally irradiated (10 Gy) and reconstituted with 100 either CCR2^{-} or CCR2^{+} CD150^{+} CD48^{-} LSK (CD45.1) and 500,000

Sca-1-depleted BM cells collected from a CD45.2 mouse. Four months after the reconstitution, mice were sacrificed and femurs were harvested. For secondary transplantation, 100 CD45.1+ $CCR2^-$ or $CCR2^+$ $CD150^+$ $CD48^-$ LSK were FACS-sorted 16 weeks after the primary transplantation and coinjected with 200,000 BM cells isolated from CD45.2 mice into lethally irradiated CD45.2 mice. Flow cytometry analysis was performed as discussed above. For limiting dilution assays (LDA) to assess numbers of functional HSC in $CCR2^+$ and $CCR2^-$ $CD150^+$ $CD48^-$ LSK subsets, we injected lethally irradiated CD45.1 mice with either 1000, 500, 250, 62 or 31 CD45.2 $CCR2^+$ or $CCR2^-$ HSC along with 500,000 CD45.1 bone marrow cells. To compare functional HSC numbers in $CCR2^{+/+}$ and $CCR2^{-/-}$ mice, lethally irradiated $CD45.1^+$ mice were injected with either 500,000, 125,000, 62,000, 31,000 or 15,000 $CCR2^{+/+}$ or $CCR2^{-/-}$ bone marrow cells ($CD45.2^+$) along with 500,000 CD45.1 bone marrow cells. Multi-lineage blood chimerism at 4 months after reconstitution was determined by flow cytometry. Multi-lineage blood chimerism of 0.1% or higher served as cut off value to determine responders. We used L-Calc (Stemcell Technologies) and ELDA softwares to calculate the frequency of functional HSC.

In vitro culture and colony forming units (CFU)

For the CFU assay, 1000 sorted $CCR2^+$ and $CCR2^-$ $CD150^+$ $CD48^-$ LSK were plated on methocult media (M3434, Stem Cell Technology). The plates were kept in an incubator with 5% CO2 at 37^{o}C. After 9 days, CFU for myeloid cells (CFU-M) were enumerated. The cells were stained and analyzed with an LSRII. For in vitro culture in liquid media, 600 $CCR2^+$ and $CCR2^-$ $CD150^+$ $CD48^-$ LSK were cultured in 100 µl of StemSpan SFEM (Stem Cell Technologies) supplemented with 20 ng/ ml SCF and 40 µl Penicillin and Streptomycin in an uncoated round bottom 96 well plate. After 7 days, the cells were stained and analyzed with an LSRII.

RNA extraction and quantification

Cells were directly sorted in extraction buffer supplied in Arcturus PicoPure RNA isolation kit (Applied Biosystem). After sorting, the buffer containing cells was frozen slowly on dry ice and

kept in -80 C until RNA extraction. RNA was extracted according to the manufacturer's protocol and eluted in a total volume of 10 µl. RNA was quantified using a ribogreen assay (Invitrogen). The RNA samples used for microarray were further analyzed using a Bioanalyzer. The RNA samples with an RNA integrity number 7.0 or more were used for microarray analysis.

Quantitative RT-PCR

Nine µl of the eluted RNA was used to generate complimentary DNA (cDNA) using a high capacity RNA to cDNA kit (Applied Biosystems). Target genes were quantified using Taqman gene expression assays (Applied Biosystems). Variability in loading different amount of cDNA was normalized using Gapdh.

Intravital microscopy (IVM)

Sorted $CCR2^{+}$ and $CCR2^{-}$ $CD150^{+}$ $CD48^{-}$ LSK were stained with 5 µM DiD (Excitation 644 nm/ emission 665 nm) and DiO (excitation 484 nm/ emission 501 nm), respectively. The stained cells were injected via tail vein into C57BL/6 recipient mice 1 day before imaging. The mice were also injected with osteosense 750 (Perkin Elmer, excitation 750 nm/ emission 780 nm) 24 hours before imaging to visualize osteoblasts lining the endosteum (Zaheer et al., 2001). Immediately prior to imaging, TRITC-dextran (excitation 544 nm/ emission 574 nm) was injected to visualize the blood pool. Cells within the skull bone marrow cavity were imaged with a confocal microscope (Olympus IV100) (Lo Celso et al., 2009) (Dutta et al., 2012). This microscope uses optics with a millimeter footprint and allows an imaging depth that extends up to 500 µm from a 1.3 mm diameter stick objective that is up to 2 cm in length. It has four laser lines: 488 nm: GFP/ FITC filter, 561 nm: Rhodamin filter, 633 nm: C5.5 filter and 748 nm: AF750, Cy7 filter. The imaging was performed with 488 and 633 nm laser illumination for DiO and DiD, respectively. Fluorescence signals from bone and blood pool were visualized using 748 nm and 561 nm laser illumination, respectively. We performed 3D analysis to measure distance between HSC and the endosteum as described previously (Lo Celso et al., 2009). Four channels were recorded: DiO

(excitation/emission 484/501 nm), DiD (excitation/emission 644/665 nm), OsteoSense 750 (excitation/emission 750/780 nm) and TRITC–Dextran (excitation/emission 557/576 nm). We generated z image stacks at 5 μm steps in z direction using Image J software. Next, we determined the focal plane where an individual HSC resided. We selected osteoblast images at the focal plane and 10, 20, 30 and 40 μm (z) away from the plane. We then combined the image of the HSC at the focal plane with the osteoblast images to measure the shortest distance (x) between the HSC and the neighboring osteoblast. The three dimensional distance (y) between the HSC and osteoblasts was calculated using $y= \sqrt{(x^2+z^2)}$. This procedure was repeated for each HSC and resulted in three-dimensional data.

PET-CT

Mice were imaged by PET-CT using an Inveon (Siemens) small animal scanner. 1 hour prior to PET imaging, mice received an IV injection of 370±100μCi ^{18}F-FLT via tail vein. CT preceded PET, acquiring 360 cone beam projections with a source power and current of 80keV and 500μA, respectively. Projections were reconstructed into three-dimensional volumes containing 512x512x768 voxels with the dimension of 0.11x0.11x0.11mm. Each PET acquisition was ~40 minutes in duration and PET images were reconstructed from 600 million coincidental, 511 keV photon counts. A high-resolution Fourier re-binning algorithm was used to re-bin sinograms, followed by a filtered back-projection algorithm for reconstruction. Image voxel size was 0.797x0.861x0.861mm. PET and CT datasets were fused and data were calculated as mean standardized uptake values (SUV) using Inveon Research Workplace Software (Siemens). Further image processing was performed using OsiriX imaging software.

Transmission Electron microscopy (TEM)

For TEM, we sorted CCR2$^+$ and CCR2$^-$ CD150$^+$ CD48$^-$ LSK in cold PBS containing 10% FBS. The cells were pelleted by centrifuging at 500g for 10 minutes. The supernatant was discarded.

Cells were fixed in 2% glutaraldehyde and given to the MGH Program in Membrane Biology microscopy core facility for standard transmission electron microscopy ultrastructural analysis.

TEM data analysis

TEM images were first filtered to reduce random noise. Multiple ROIs were then manually selected within each cell's cytoplasm, and ribosome coordinates were detected within the ROIs using a morphology-based segmentation method. Automated detection was followed by visual inspection with subsequent correction for erroneous assignment and data rejection. The Hopkins index H was then computed for all ribosome coordinates as a numerical indicator for clustering tendency (Zhang et al., 2006). Its value in a two-dimensional space relies on computation of Euclidean distances between m ribosomes r_k (k=1..m) randomly chosen from a set S_R (dim S_R = N), and m randomly chosen points p_i (i=1..m) from a set S' (dim S' = N) according to

$$H = \frac{\sum_{i=1}^{m} u_i^2}{\sum_{i=1}^{m} u_i^2 + \sum_{k=1}^{m} w_k^2}$$

where u_i is the minimum distance between a random point p_i and all ribosomes r_k ($\forall r_k \in S_R$) and w_k is the minimum distance between a ribosome r_k and all its neighbors. The H index can take values between 0 and 1. A value of H approximating 0 indicates an even spatial distribution while a value approaching 1 indicates an increasing probability of clustering. At 0.75, a clustering tendency at 90% confidence level is present. Within each image two to three ROIs were selected and up to 200 points per ROI were considered.

Fluorescence Molecular Tomography-Computed Tomography (FMT/CT). Mice were injected with a pan-cathepsin protease sensor (Prosense-680, PerkinElmer, 5 nmol). Protease activity was measured in hearts 7d after MI by utilizing fluorescence molecular tomography (FMT) in combination with computed tomography (CT) as described previously (Nahrendorf et

al., 2009).

Magnetic resonance imaging (MRI). Cardiac MRI was performed on day 1 and 21 after permanent coronary ligation as described perviously (Courties et al., 2014). Cine images of the left ventricular short axis were acquired by using a 7 Tesla horizontal bore Pharmascan (Bruker) and a custom-built mouse cardiac coil (Rapid Biomedical). Acquisition and analysis was carried out as described previously (Courties et al., 2014).

Immunohistochemistry. Hearts were embedded in O.C.T. compound (Sakura Finetek) and immediately snap-frozen in a dry ice cooled 2-methylbutane. Five µm frozen sections were prepared and then stained using antibodies against alpha-smooth muscle actin (αSMA, Abcam, clone ab5694), collagen I (Abcam, clone ab21286), CD31 (BD Biosciences, clone MEC13.3) and CD68 (AbD Serotec, clone FA-11). We subsequently applied biotinylated secondary antibodies and the used the VECTASTAIN ABC kit (Vector Laboratories, Inc.). Color development was carried out by using an AEC substrate (Dako), sections were counterstained with hematoxylin eosin. Slides were digitalized using a Nanozoomer 2.0RS scanner (Hamamatsu, Japan), and the positive area quantified using IPLab (version 3.9.3; Scanalytics, Inc.). We analyzed 12-20 high-power fields per section and per animal.

Supplemental References

Courties, G., Heidt, T., Sebas, M., Iwamoto, Y., Jeon, D., Truelove, J., Tricot, B., Wojtkiewicz, G., Dutta, P., Sager, H. B., Borodovsky, A., Novobrantseva, T., Klebanov, B., Fitzgerald, K., Anderson, D. G., Libby, P., Swirski, F. K., Weissleder, R., and Nahrendorf, M. (2014). In vivo silencing of the transcription factor IRF5 reprograms the macrophage phenotype and improves infarct healing. J Am Coll Cardiol *63*, 1556-1566.

Dutta, P., Courties, G., Wei, Y., Leuschner, F., Gorbatov, R., Robbins, C. S., Iwamoto, Y., Thompson, B., Carlson, A. L., Heidt, T., Majmudar, M. D., Lasitschka, F., Etzrodt, M., Waterman, P., Waring, M. T., Chicoine, A. T., van der Laan, A. M., Niessen, H. W., Piek, J. J., Rubin, B. B., Butany, J., Stone, J. R., Katus, H. A., Murphy, S. A., Morrow, D. A., Sabatine, M. S., Vinegoni, C., Moskowitz, M. A., Pittet, M. J., Libby, P., Lin, C. P., Swirski, F. K., Weissleder, R., and Nahrendorf, M. (2012). Myocardial infarction accelerates atherosclerosis. Nature *487*, 325-329.

Lo Celso, C., Fleming, H. E., Wu, J. W., Zhao, C. X., Miake-Lye, S., Fujisaki, J., Cote, D., Rowe, D. W., Lin, C. P., and Scadden, D. T. (2009). Live-animal tracking of individual haematopoietic stem/progenitor cells in their niche. Nature *457*, 92-96.

Nahrendorf, M., Waterman, P., Thurber, G., Groves, K., Rajopadhye, M., Panizzi, P., Marinelli, B., Aikawa, E., Pittet, M. J., Swirski, F. K., and Weissleder, R. (2009). Hybrid in vivo FMT-CT imaging of protease activity in atherosclerosis with customized nanosensors. Arterioscler Thromb Vasc Biol *29*, 1444-1451.

Pang, W. W., Price, E. A., Sahoo, D., Beerman, I., Maloney, W. J., Rossi, D. J., Schrier, S. L., and Weissman, I. L. (2011). Human bone marrow hematopoietic stem cells are increased in frequency and myeloid-biased with age. Proc Natl Acad Sci U S A *108*, 20012-20017.
Zaheer, A., Lenkinski, R. E., Mahmood, A., Jones, A. G., Cantley, L. C., and Frangioni, J. V. (2001). In vivo near-infrared fluorescence imaging of osteoblastic activity. Nat Biotechnol *19*, 1148-1154.

Zhang, J., Leiderman, K., Pfeiffer, J. R., Wilson, B. S., Oliver, J. M., and Steinberg, S. L. (2006). Characterizing the topography of membrane receptors and signaling molecules from spatial patterns obtained using nanometer-scale electron-dense probes and electron microscopy. Micron *37*, 14-34.